Surface Chemistry

International Edition: DOI: 10.1002/anie.201602414
German Edition: DOI: 10.1002/ange.201602414

Catalytic Dealkylation of Ethers to Alcohols on Metal Surfaces

Biao Yang[+], Haiping Lin[+], Kangjian Miao, Pan Zhu, Liangbo Liang, Kewei Sun, Haiming Zhang, Jian Fan, Vincent Meunier, Youyong Li, Qing Li, and Lifeng Chi**

Abstract: *On-surface synthesis has prompted much interest in recent years because it provides an alternative strategy for controlling chemical reactions and allows for the direct observation of reaction pathways. Herein, we combined scanning tunneling microscopy and density functional theory to provide extensive evidence for the conversion of alkoxybenzene-containing ethers into alcohols by means of surface synthesis. The reported dealkylation reactions are finely controlled by the annealing parameters, which govern the onset of successive alkyl chains dissociations. Moreover, density functional theory calculations elucidate the details of the reaction pathways, showing that dealkylation reactions are surface-assisted and very different from their homogeneous analogues in solution.*

Understanding and controlling chemical reactions at the single molecule level has spurred much interest over the past few years. The development of on-surface chemistry, which combines mostly ultrahigh vacuum (UHV) and scanning tunneling microscopy (STM) techniques, provides ideal tools to promote the understanding of physical and chemical processes governing the on-surface reactions.[1–14] Local probe analysis enables the monitoring of both reactants and products at the single-molecule-scale on selected substrates, thereby aiding in the identification of the characteristics of reaction pathways. This approach is also an ideal platform for developing a strategy for the controlled structural evolution on surfaces through on-surface chemical reactions.

On-surface reactions can be triggered by a probe tip,[15–17] UV excitation,[18] or appropriate annealing.[19] To date, various types of reactions have been performed on supported surfaces, such as the Ullmann reaction,[19,20] Glaser coupling,[21] azide–alkyne cycloaddition,[22] and imine formation.[23,24] Using these techniques, various covalent connected supramolecular structures were constructed on surfaces, including graphene nanoribbons with precise edge shapes, sizes,[20,25–28] or chemical doping,[29,30] and two-dimensional porous networks.[31] Moreover, due to the unique space confinement and the catalytic ability of the surface, one should be able to realize certain types of reactions that are difficult to complete using traditional approaches, such as dehydrogenative coupling of alkanes on a reconstructed Au(110) surface.[32]

Most efforts of surface reaction are devoted to the bottom-up synthesis of covalent networks. However, the types of chemical reactions reported on surfaces are still limited. Herein, we studied the thermally triggered dealkylation of ethers, which proceeds via the scission of C–O bonds on various metal surfaces. The cleavage of C–O bonds in alkoxybenzene-containing ethers is considered to be one of the important type of reactions because of its capability to produce alcohols, particularly in deprotection reactions. Traditionally, dealkylation reactions are conducted in the presence of protic acids (such as HBr) or Lewis acids (such as boron tribromide) used as catalysts.[33,34] In our present work, STM observations revealed the distinct phase evolutions of diol and triol as the substrate temperature increased. We combined the experimental studies with density functional theory (DFT) calculations to provide unambiguous evidence that the reaction products are alcohol derivatives. The dealkylation process was found to be controlled by the annealing parameters (temperature and time), which prompt the successive steps of alkyl chain dissociation. We systematically studied the reaction characteristics of different alkoxybenzene derivatives on Au(111), Ag(111), and Cu(111) surfaces, respectively, and found that the dealkylation of these compounds is a general process occurring on these metal surfaces. Moreover, the reaction pathway was elucidated by the extensive DFT calculations, which showed a key role of surface metal ad-atoms during the reaction.

Figure 1a displays a representative STM image after the initial deposition of the 1,3,5-tris(4-Dodecyloxyphenyl)benzene (TDPB) on a Au(111) substrate held at room temperature. The corresponding structural model of TDPB is shown in the inset of Figure 1a. The TDPB molecules self-assemble into a perfectly periodic network structure, extending defect-free over a large surface area. A closer inspection of the ordered structure reveals that the molecules exhibit a planar configuration (Figure S1a). The triangular-shaped objects represent the 1,3,5-triphenylbenzene cores, while the atomically resolved elongated stripes in Figure S1a correspond to the alkoxy chains. Thus, the porous structure is stabilized by van der Waals interactions between the parallel alkyl chains, which is reminiscent of the self-assembly behaviors of alkoxybenzene derivatives.[35] The right panels of Figure 1a show the DFT optimized geometry and the simulated STM

[*] B. Yang,[+] H. P. Lin,[+] K. J. Miao, K. W. Sun, Dr. H. M. Zhang, Dr. J. Fan, Prof. Y. Y. Li, Dr. Q. Li, Prof. L. F. Chi
Institute of Functional Nano and Soft Materials (FUNSOM)
Jiangsu Key Laboratory for Carbon-Based Functional Materials & Devices
Soochow University
Suzhou 215123 (P.R. China)
E-mail: liqing@suda.edu.cn
chilf@suda.edu.cn
P. Zhu, L. B. Liang, Prof. V. Meunier
Department of Physics, Applied Physics, and Astronomy
Rensselaer Polytechnic Institute
Troy, NY 12180 (USA)
[+] These authors contributed equally to this work.

Supporting information for this article can be found under: http://dx.doi.org/10.1002/anie.201602414.

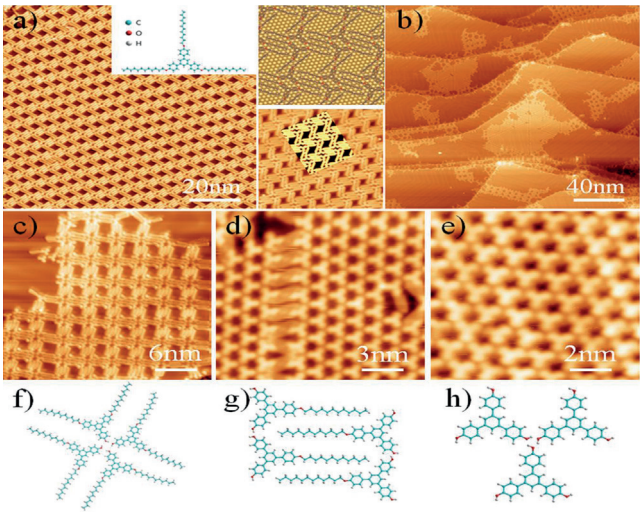

Figure 1. a) Self-assembled structure after the initial adsorption of TDPB molecules on Au(111) substrate. Left panel shows the representative STM image. The inset of left panel shows the structural model of TDPB. Upper right and lower right panels show the DFT relaxed model and the simulated STM image, respectively. b) Representative STM image after annealing at 140 °C for 15 minutes. c–e) High resolution images of three kinds of islands. f–h) Structural models of the self-assembled structures shown in (c–e).

image of the self-assembly structure. The experimental STM image is in excellent agreement with the simulated image, which further supports the proposed structural model shown in Figure 1 a. Note that although the constitutive TDPB molecule displays high symmetry, the overall self-assembly structure is chiral owing to the directional interactions (Figure S1).[36]

The resulting networked structure was quite robust as it remained unchanged up to 140 °C. However, upon annealing the sample at 140 °C for 15 minutes, a dramatic phase evolution was observed, in which the molecules aggregate into several isolated islands (Figure 1 b). To investigate the details of these structures, we acquired high-resolution images of each phase (Figure 1 c–e). In Figure 1 c, the island presents an overall square shape. High-resolution image reveals that each TDPB molecule in this phase (A phase) has one alkyl chain missing and the newly-formed terminals point to a specific center (Figure 1 f). The two remaining alkyl chains remain parallel to the adjacent chains. The B phase (Figure 1 d and 1 g) is characterized by the presence of domain boundaries between two triangular islands. In this phase, each TDPB molecule has two dissociated alkyl chains. The third observed phase (C phase) is the most close-packed structure (Figure 1 e and 1 h). In this phase, all of the alkyl chains are dissociated and the self-assembly structure is held together by a network of hydrogen bonds extending between the tentatively assigned hydroxyls of the products (further analysis of this structure can be found in Figure 2). It is worth noting that we did not observe dissociated alkyl chains (C_{12}) on the STM images. This can be explained by their low adsorption energies on the Au(111),[37] leading to their desorption during annealing.

To elucidate the successive dealkylation processes and the resulting phase evolution, a series of temperature-dependent experiments were conducted (Figure S2). Statistical analysis (Figure 2 a) revealed that the carbon chains dissociate successively upon thermal activation. When the temperature increases up to 180 °C, only C phase islands can be observed on the surface, suggesting that almost all the alkyl chains are dissociated. Note that the C phase is very robust and the structure remains unaltered up to 230 °C.

STM images suggested the occurrence of the reaction within the scanning area. The evidence of carbon chain dissociation on the entire surface was given by X-ray photoelectron spectroscopy (XPS) measurements. We obtained the C1s and O1s spectrum both after initial deposition and 180 °C annealing for 10 mins (Figure 2 b). The distinct peak shifts in both the C1s and O1s signals suggest a structural evolution after annealing (see the Supporting Information for details). Additionally, we calculated the area covered by each spectrum to gain insight into the number of carbon and oxygen atoms involved in the process. We found that the carbon-to-oxygen ratio after initial deposition is 1.7-times the ratio after annealing at 180 °C for 10 minutes. The significant loss of carbon strongly suggests the dealkylation reaction through the thermal activation. Note that the carbon-to-oxygen ratio of pristine TDPB molecules is 2.5-times greater than the ratio after all of the carbon chains have been dissociated.

In solution, the dealkylation of alkoxybenzene-based ethers generate phenol derivatives,[33,34] which is in good agreement with the fact that the strong oxygen signal (Figure 2 b) in the XPS spectra suggests the oxygen atoms remain in the benzene side after reaction. To further validate our hypothesis, we obtained the DFT optimized self-assembly structure of 1,3,5-tris(4-hydroxyphenyl)benzene (THPB; Figure 2 c) and the corresponding simulated STM image (inset of Figure 2 d). Both are in excellent agreement with the experimental observations (Figure 2 c and 2 d). Note that the hydroxy groups of the proposed products result in a pinwheel-shaped hydrogen bonding pattern between the mole-

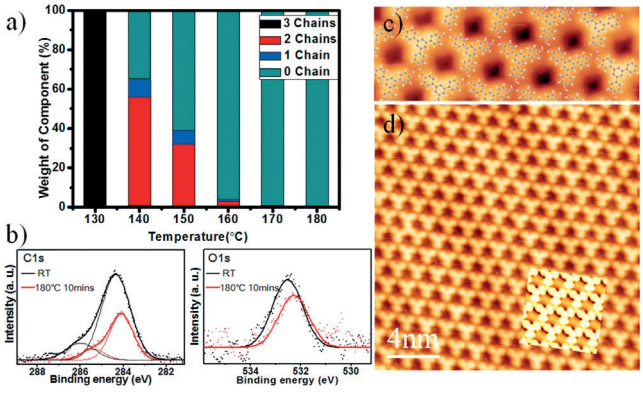

Figure 2. a) Statistical diagram based on Figure S2, showing the distribution of four kinds of molecules with 0, 1, 2, and 3 carbon chains remaining at each stage. b) C1s and O1s XPS spectra of the sample after initial deposition and 180 °C annealing. c) STM image superposed with the relaxed self-assembly model of the proposed reaction products. d) Experimental and simulated STM images. The calculated image is based on the model shown in (c).

cules. This explains why such an ordered structure is so robust and remains stable at up to 230 °C. To further confirm the reaction products, we synthesized the hypothesized product THPB molecules and studied their self-assembling behaviors on Au(111) surfaces. The self-assembled structures of THPB on Au(111) are exactly the same to that in Figure 2 d, thereby confirming the proposed reaction model unambiguously[38] (details can be found in Figure S3).

The observed reactions are not only valid for TBPB reactants, but also work for other ether derivative with different symmetry (Figure S4), showing the universality of the dealkylation of alkoxybenzene-containing ethers on Au(111). In solution, the dealkylation of ethers requires either protic acids (for example, HBr) or Lewis acids (for example, BBr_3) as catalysts.[33,34] Because no acid is involved in our experiments, the alkyl dissociations we observed here are surface-assisted. First-principles Climbing Image Nudge-Elastic Band (CI-NEB) calculations were performed to understand the reaction mechanisms of such C–O bond scission reactions. To increase the computational efficiency, the TDPB molecule was modeled with a phenyl propyl ether molecule. As shown in Figure 3, in the initial state (IS),

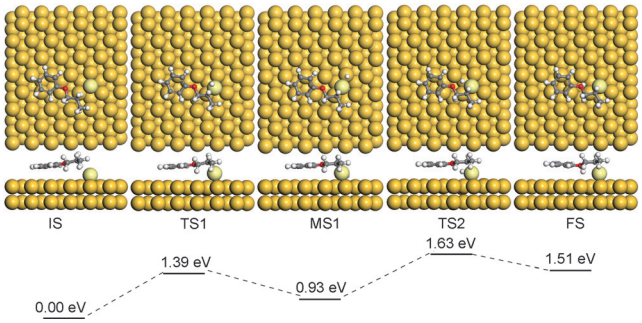

Figure 3. Reaction pathway and the energy profiles in the C–O bond scission reaction. The Au, C, O, and H atoms are represented by yellow, gray, red, white circles, respectively. The Au ad-atom is represented with a circle colored in pale yellow.

a phenyl propyl ether molecule adsorbs on a Au(111) surface, with a Au ad-atom sitting above a hollow site next to the propyl group. The Au ad-atom is involved in this catalytic C–O bond scission reaction for two reasons: 1) The existence of ad-atoms on metal surfaces is well accepted and the catalytic behavior of metal ad-atoms has been wildly reported.[2] 2) We have performed DFT calculations for two alternative reaction pathways without the presence of Au ad-atoms (Figure S5 and Figure S6), and found that the corresponding activation barriers, are much higher than the experimental observations. In the first transition state (TS1), one of the C–H bonds of the propyl group is dissociated (the distance between the C atom and H atom is elongated from 1.11 Å to 2.03 Å). The dissociated hydrogen atom is stabilized by the Au ad-atom (the H–Au bond length is 1.59 Å). Passing over TS1, the hydrogen atom moves across the Au ad-atom and bonds to the Au substrate and the Au ad-atom, resulting in a meta-state (MS). The activation energy of such a dehydrogenation process is 1.39 eV. As the hydrogen atom is quite active and mobile on the Au(111) surface, it may diffuse toward the O atom and result in the formation of an alcohol. In the second transition state (TS2), the O–H bond length is 1.26 Å, and the Au–H bond length is 1.78 Å. In the final state (FS), a new O–H bond is formed (O–H distance is 1.02 Å), and the O–C bond is elongated from 1.43 Å to 1.56 Å. The activation barrier of MS to FS is 0.70 eV. The final products are, therefore, a phenol molecule and a propylene molecule co-adsorbed on the Au ad-atom. The subsequent diffusion of the propylene molecules away from the Au ad-atom requires to overcome a small activation barrier of 0.12 eV. Correspondingly, the total energy will be decreased by 1.55 eV (Figure S7). Thus, the C–O bond scission reaction consists of two elementary processes. The energy profiles are illustrated in the lower panel of Figure 3, which shows that the Au ad-atom plays a key role in stabilizing the transition states in both elementary processes. The dehydrogenation process is the rate-limiting-step, and the overall energy barrier of the C–O bond scission process is therefore 1.39 eV. One should also note that from the thermal dynamical point of view, the split-off hydrogen or the adsorbed hydrogen atoms may also react with the C atom that attached to the Au ad-atom, resulting in the inversed reaction from the MS1 state to the IS state. The reaction pathway proposed here is our best assumption that accounts for the experimental observations. More alternative reaction pathways should be further investigated to unambiguously reveal the reaction mechanism.

To gain further insight into the role of the surface, we reproduced the reactions on other metal surfaces, such as Ag(111) and Cu(111) (Figure S8). Our results make it clear that the dealkylation of ethers is not only valid on Au(111) surface, but is also applicable for other metal surfaces. We recorded the temperatures that needed to trigger the dissociation reactions for both TDPB and DHQP on Au(111), Ag(111), and Cu(111), respectively, and listed them in Table S1. It is quite interesting that the difference in reaction temperatures for both molecules on a specific substrate is almost negligible. A similar reaction temperature on a specific surface is also supported by co-adsorption of TDPB and DHQP on Au (111) surfaces (Figure S9). In contrast, the reaction temperatures vary significantly on different substrates. Specifically, the dealkylation can occur at close to room temperature on Cu(111) surface, for both TDPB and DHQP molecules, suggesting that the copper surface has stronger catalytic ability when compared with silver and gold surfaces, in agreement with experimental results reported elsewhere.[3]

In conclusion, the thermal stability of alkoxy chains was systematically studied with two alkoxylated molecules, TDPB and BHQP, on different metal surfaces. We found that the C–O bond breaks at elevated temperatures, resulting in dealkylation on various metal surfaces. Combining STM imaging and DFT calculations, we provided evidence that the product of the dealkylation reaction display hydroxy terminals. Moreover, we show that the dealkylation can be well controlled by tuning the annealing parameters. Self-assembly of intact molecules, intermediates, and final products observed with STM allow us to follow the structural evolution before, during, and after the reactions to help deduce the molecular

structures at each stage. Our studies provide an alternative strategy for dealkylation reactions other than the typical acid-assisted reaction. We envision that, in the future, excitation with light or local electron/hole injection may also be used to trigger the dissociation reaction, paving the way to a better understanding of the reaction principles of dealkylation of alkoxybenzene-containing ethers.

Experimental Section

Sample preparation and STM measurements were performed in an ultrahigh vacuum system (base pressure is better than 1×10^{-10} torr). Experiments were conducted with a commercial Unisoku low-temperature scanning tunneling microscopy. All of the STM measurements were performed at 77 K. The Au(111), Ag(111), and Cu(111) surfaces were cleaned by standard argon sputtering–annealing cycles before deposition of organic molecules. A commercial Pt-Ir tip was carefully prepared by e-beam heating. The STM images were analyzed using WsXM.

Acknowledgements

We thank Prof. D. H. Yan and Prof. H. B. Wang for the help in XPS measurements. We acknowledge Collaborative Innovation Center of Suzhou Nano Science & Technology, the Priority Academic Program Development of Jiangsu Higher Education Institutions. This work was supported by the NSFC (Nos. 91227201, 91545127 , 21403149), Major State Basic Research Development Program of China (No. 2014CB932600), and the Natural Science Foundation of Jiangsu Province (Nos. BK20140305 and BK20150305). Work at RPI was supported by the US Office of Naval Research. Calculations were partially performed on Rensselaer Center for Computational Innovations.

Keywords: dealkylation · density functional theory · on-surface reactions · scanning tunneling microscopy · surface chemistry

How to cite: *Angew. Chem. Int. Ed.* **2016**, *55*, 9881–9885
Angew. Chem. **2016**, *128*, 10035–10039

[1] N. A. A. Zwaneveld, R. Pawlak, M. Abel, D. Catalin, D. Gigmes, D. Bertin, L. Porte, *J. Am. Chem. Soc.* **2008**, *130*, 6678–6679.
[2] Q. Li, B. Yang, H. P. Lin, N. Aghdassi, K. J. Miao, J. J. Zhang, H. M. Zhang, Y. Y. Li, S. Duhm, J. Fan, L. F. Chi, *J. Am. Chem. Soc.* **2016**, *138*, 2809–2814.
[3] G. Franc, A. Gourdon, *Phys. Chem. Chem. Phys.* **2011**, *13*, 14283–14292.
[4] M. Abel, S. Clair, O. Ourdjini, M. Mossoyan, L. Porte, *J. Am. Chem. Soc.* **2011**, *133*, 1203–1205.
[5] T. Lin, X. S. Shang, J. Adisoejoso, P. N. Liu, N. Lin, *J. Am. Chem. Soc.* **2013**, *135*, 3576–3582.
[6] B. Yang, J. Bjork, H. P. Lin, X. Q. Zhang, H. M. Zhang, Y. Y. Li, J. Fan, Q. Li, L. F. Chi, *J. Am. Chem. Soc.* **2015**, *137*, 4904–4907.
[7] A. Gourdon, *Angew. Chem. Int. Ed.* **2008**, *47*, 6950–6953; *Angew. Chem.* **2008**, *120*, 7056–7059.
[8] H. T. Zhou, J. Z. Liu, S. X. Du, L. Z. Zhang, G. Li, Y. Zhang, B. Z. Tang, H. J. Gao, *J. Am. Chem. Soc.* **2014**, *136*, 5567–5570.
[9] X. M. Zhang, L. Y. Liao, S. Wang, F. Y. Hu, C. Wang, Q. D. Zeng, *Sci. Rep.* **2014**, *4*, 3899.
[10] L. Y. O. Yang, C. Z. Chang, S. H. Liu, C. G. Wu, S. L. Yau, *J. Am. Chem. Soc.* **2007**, *129*, 8076–8077.
[11] M. Matena, T. Riehm, M. Stöhr, T. A. Jung, L. H. Gade, *Angew. Chem. Int. Ed.* **2008**, *47*, 2414–2417; *Angew. Chem.* **2008**, *120*, 2448–2451.
[12] D. F. Perepichka, F. Rosei, *Science* **2009**, *323*, 216–217.
[13] Q. T. Fan, C. C. Wang, Y. Han, J. F. Zhu, W. Hieringer, J. Kuttner, G. Hilt, J. M. Gottfried, *Angew. Chem. Int. Ed.* **2013**, *52*, 4668–4672; *Angew. Chem.* **2013**, *125*, 4766–4770.
[14] X. H. Liu, C. Z. Guan, S. Y. Ding, W. Wang, H. J. Yan, D. Wang, L. J. Wan, *J. Am. Chem. Soc.* **2013**, *135*, 10470–10474.
[15] S. W. Hla, L. Bartels, G. Meyer, K. H. Rieder, *Phys. Rev. Lett.* **2000**, *85*, 2777–2780.
[16] Q. Li, C. B. Han, M. Fuentes-Cabrera, H. Terrones, B. G. Sumpter, W. C. Lu, J. Bernholc, J. Y. Yi, Z. Gai, A. P. Baddorf, P. Maksymovych, M. H. Pan, *ACS Nano* **2012**, *6*, 9267–9275.
[17] Q. Li, J. R. Owens, C. B. Han, B. G. Sumpter, W. C. Lu, J. Bernholc, V. Meunier, P. Maksymovych, M. Fuentes-Cabrera, M. H. Pan, *Sci. Rep.* **2013**, *3*, 2102.
[18] H. Y. Gao, D. Y. Zhong, H. Moenig, H. Wagner, P. A. Held, A. Timmer, A. Studer, H. Fuchs, *J. Phys. Chem. C* **2014**, *118*, 6272–6277.
[19] L. Grill, M. Dyer, L. Lafferentz, M. Persson, M. V. Peters, S. Hecht, *Nat. Nanotechnol.* **2007**, *2*, 687–691.
[20] J. M. Cai, P. Ruffieux, R. Jaafar, M. Bieri, T. Braun, S. Blankenburg, M. Muoth, A. P. Seitsonen, M. Saleh, X. L. Feng, K. Müllen, R. Fasel, *Nature* **2010**, *466*, 470–473.
[21] Y. Q. Zhang, N. Kepčija, M. Kleinschrodt, K. Diller, S. Fischer, A. C. Papageorgiou, F. Allegretti, J. Björk, S. Klyatskaya, F. Klappenberger, M. Ruben, J. V. Barth, *Nat. Commun.* **2012**, *3*, 1286.
[22] O. Díaz Arado, H. Monig, H. Wagner, J. H. Franke, G. Langewisch, P. A. Held, A. Studer, H. Fuchs, *ACS Nano* **2013**, *7*, 8509–8515.
[23] S. Weigelt, C. Busse, C. Bombis, M. M. Knudsen, K. V. Gothelf, T. Strunskus, C. Wöll, M. Dahlbom, B. Hammer, E. Lægsgaard, F. Besenbacher, T. R. Linderoth, *Angew. Chem. Int. Ed.* **2007**, *46*, 9227–9230; *Angew. Chem.* **2007**, *119*, 9387–9390.
[24] S. Weigelt, C. Busse, C. Bombis, M. M. Knudsen, K. V. Gothelf, E. Lægsgaard, F. Besenbacher, T. R. Linderoth, *Angew. Chem. Int. Ed.* **2008**, *47*, 4406–4410; *Angew. Chem.* **2008**, *120*, 4478–4482.
[25] S. Linden, D. Y. Zhong, A. Timmer, N. Aghdassi, J. H. Franke, H. M. Zhang, X. L. Feng, K. Mullen, H. Fuchs, L. F. Chi, H. Zacharias, *Phys. Rev. Lett.* **2012**, *108*, 216801.
[26] Y. C. Chen, D. G. de Oteyza, Z. Pedramrazi, C. Chen, F. R. Fischer, M. F. Crommie, *ACS Nano* **2013**, *7*, 6123–6128.
[27] H. M. Zhang, H. P. Lin, K. W. Sun, L. Chen, Y. Zagranyarski, N. Aghdassi, S. Duhm, Q. Li, D. Y. Zhong, Y. Y. Li, K. Mullen, H. Fuchs, L. F. Chi, *J. Am. Chem. Soc.* **2015**, *137*, 4022–4025.
[28] P. Ruffieux, S. Y. Wang, B. Yang, C. Sanchez-Sanchez, J. Liu, T. Dienel, L. Talirz, P. Shinde, C. A. Pignedoli, D. Passerone, T. Dumslaff, X. L. Feng, K. Mullen, R. Fasel, *Nature* **2016**, *531*, 489.
[29] C. Bronner, S. Stremlau, M. Gille, F. Brauße, A. Haase, S. Hecht, P. Tegeder, *Angew. Chem. Int. Ed.* **2013**, *52*, 4422–4425; *Angew. Chem.* **2013**, *125*, 4518–4521.
[30] J. M. Cai, C. A. Pignedoli, L. Talirz, P. Ruffieux, H. Söde, L. B. Liang, V. Meunier, R. Berger, R. J. Li, X. L. Feng, K. Müllen, R. Fasel, *Nat. Nanotechnol.* **2014**, *9*, 896–900.
[31] M. Bieri, M. T. Nguyen, O. Gröning, J. Cai, M. Treier, K. Aït-Mansour, P. Ruffieux, C. A. Pignedoli, D. Passerone, M. Kastler, K. Müllen, R. Fasel, *J. Am. Chem. Soc.* **2010**, *132*, 16669–16676.
[32] D. Y. Zhong, J. H. Franke, S. K. Podiyanachari, T. Blömker, H. M. Zhang, G. Kehr, G. Erker, H. Fuchs, L. F. Chi, *Science* **2011**, *334*, 213–216.
[33] I. Ryu, H. Matsubara, S. Yasuda, H. Nakamura, D. P. Curran, *J. Am. Chem. Soc.* **2002**, *124*, 12946–12947.

[34] A. Leyva-Pérez, D. Combita-Merchan, J. R. Cabrero-Antonino, S. I. Al-Resayes, A. Corma, *ACS Catal.* **2013**, *3*, 250 – 258.
[35] M. O. Blunt, J. Adisoejoso, K. Tahara, K. Katayama, M. Van der Auweraer, Y. Tobe, S. De Feyter, *J. Am. Chem. Soc.* **2013**, *135*, 12068 – 12075.
[36] Q. Li, C. B. Han, S. R. Horton, M. Fuentes-Cabrera, B. G. Sumpter, W. C. Lu, J. Bernholc, P. Maksymovych, M. H. Pan, *ACS Nano* **2012**, *6*, 566 – 572.
[37] K. R. Paserba, A. J. Gellman, *J. Chem. Phys.* **2001**, *115*, 6737 – 6751.
[38] A. C. Marele, I. Corral, P. Sanz, R. Mas-Balleste, F. Zamora, M. Yanez, J. M. Gomez-Rodriguez, *J. Phys. Chem. C* **2013**, *117*, 4680 – 4690.

Received: March 9, 2016
Revised: June 18, 2016
Published online: July 19, 2016

